

# Small Animal Simulation Studies using the microPET® FOCUS System and the GATE Platform

S. Branco<sup>1</sup>, P. Almeida<sup>1</sup> & S. Jan<sup>2</sup>

<sup>1</sup>Universidade de Lisboa, Faculdade de Ciências, Instituto de Biofísica e Engenharia Biomédica, Portugal

<sup>2</sup>CEA/DSV/FBM, Service Hospitalier Frédéric Joliot, France

---

*GATE, a Monte Carlo simulation platform dedicated to nuclear medicine, has been validated for modeling  $\mu$ PET systems like the microPET® FOCUS 220 under realistic imaging conditions. In this paper, the use of the microPET® FOCUS 220 simulation model with GATE is used along with realistic mouse phantoms (including respiratory motion) and radioactive distribution maps, obtained from real exams, to produce simulated PET data of a mouse. We present results from simulated realistic whole body studies of the mouse with [<sup>18</sup>F]fluoride and 2-Deoxy-[<sup>18</sup>F]fluoro-D-glucose (FDG) and compare them to real data. The simulations were performed using voxelized mouse phantoms, obtained from real PET examinations and from digital mouse anatomical models. Respiratory motion is introduced in the simulation process. The qualitative and quantitative results from simulated data reproduce real values within 23%. This discrepancy can be related with specificities of simulated and real data, in particular due to attenuation and scattering corrections.*

**Keywords:** Monte Carlo method; GATE; microPET® FOCUS; small animal; PET imaging

---

## 1. INTRODUCTION

Animal models of human diseases are a widely used research tool to understand the progress of diseases and to evaluate potential therapies and new drugs (Cherry, S. R. & Gambhir, S. S. 2001) (Luanne, L. P. *et al.* 2007). The use of animal models has recently gained increased interest due to the availability of *in vivo* small animal imaging and to the rapid growth in genetics and molecular biology (Phelps, M. E. 2000) (Cherry, S. R. & Gambhir, S. S. 2001).

Positron Emission Tomography (PET) is a non-invasive nuclear medicine technique allowing the measurement of the spatial and temporal distribution of radiotracers which map physiological and metabolic functions of the body (Wernick, M. N. & Aarsvold, J. N. 2004). Since biochemical changes precede morphologic changes, PET has the potential to provide diagnostic information earlier than, for example, X-Ray Computed Tomography (CT) or Magnetic Resonance Imaging (MRI) (Gambhir, S. S. 2002).

The use of PET in small animals allows the use of subjects as their own control, reducing the interanimal variability. This allows performing longitudinal studies on the same animal and improves the accuracy of biological models. Small animal PET is becoming very useful in several fields of molecular imaging such as the development of techniques to measure endogenous and reporter gene expression *in vivo*. Moreover, the ability of small animal PET to map the *in vivo* biodistribution of new pharmaceuticals opens up new possibilities for research using small animal models of human diseases (Cherry, S. R. & Gambhir, S. S. 2001) (Cherry, S. 2004). However, small animal PET still suffers from several limitations. In fact, the amounts of injected dose needed, limited scanner sensitivity,

image resolution and image quantification issues (Chatziioannou, A. F. 2002) (Tai, Y. C. & Laforest, R. 2005), could clearly benefit from additional research.

The simulation of small animal imaging using Monte Carlo allow modeling imaging systems, developing and assessing of tomographic image reconstruction algorithms and evaluating correction methods for improved image quantification (Andreo, P. 1991) (Zaidi, H. 1999). In this context, Monte Carlo simulations are becoming an essential tool for assisting this research and some specific Monte Carlo simulation packages have been evaluated for nuclear medicine applications (Buvat, I. & Castiglioni, I. 2002) (Buvat, I. *et al.* 2005). Recently, the Geant4 Application for Tomographic Emission (GATE) platform has been developed (Jan, S. *et al.* 2004) and validated for the simulation of the microPET® FOCUS 220 system (Jan, S. *et al.* 2005).

An important aspect of simulation is to have a realistic model (phantom) of the subject's anatomy and physiological functions from which imaging data can be generated using accurate models of the imaging process. The advantage in using such phantoms in simulation studies is that the exact anatomy and physiological functions are known. Moreover, computer phantoms can be altered in order to model different anatomies and pathological situations.

Among the most important radiotracers available for PET imaging are [<sup>18</sup>F]fluoride and 2-Deoxy-[<sup>18</sup>F]fluoro-D-glucose. The [<sup>18</sup>F]fluoride is a radiotracer with high affinity to bone structures. This radiopharmaceutical can be useful in the clinical setting. In fact, many common cancers types (*e.g.* prostate, breast and lung cancers) may originate bone metastases which result in pathological changes in bone metabolism (Berger, F. *et al.* 2002) (Couturier, O. 2004). The FDG is the most common radiotracer used for cancer

imaging in PET. FDG is an analog of glucose and is taken up by living cells through the normal glucose pathway. Tumor imaging with FDG relies on the fact that malignant cells possess high metabolic rates and therefore take up greater amounts of FDG than healthy tissues (Couturier, O. 2004) (Larson, S. M. & Schwartz, L. H. 2006).

In this paper we reports on the use of GATE for producing realistic simulated data of [ $^{18}\text{F}$ ]fluoride and FDG distribution in the mouse body using the microPET<sup>®</sup> FOCUS 220 system. We build on previously published work (Branco, S. *et al.* 2007a), (Branco, S. *et al.* 2007b), (Branco, S. *et al.* 2007c) to introduce time dependence as a new feature dealt with small animal imaging simulations using GATE.

## 2. MATERIAL AND METHODS

### 2.1 The MicroPET<sup>®</sup> FOCUS 220 System

The microPET<sup>®</sup> FOCUS 220 system is a commercial scanner consisting in 4 detector rings: each ring is made of 42 detector blocks. Each detector block is composed of a matrix of  $12 \times 12$  LSO crystals with the dimensions  $1.5 \text{ mm} \times 1.5 \text{ mm} \times 10.0 \text{ mm}$ . Its axial Field of View (FOV) is 7.6 cm and has a diameter of 26.0 cm. The FOCUS system has a volume resolution of  $2.5 \mu\text{L}$  and an absolute sensitivity of 3.4 %, both measured at the center of the FOV (Tai, Y. *et al.* 2005). The system is suitable for acquiring high resolution images of small animal as rodents (mice and rats) and primates (macaque and small baboon).

### 2.2 The GATE Platform

GATE (<http://www.opengatecollaboration.org>) is a generic Monte Carlo simulation platform based on Geant4 libraries and dedicated to nuclear medicine imaging (Agostinelli, S. *et al.* 2003). GATE includes specific features allowing the management of time-dependent processes such as detector and patient movements, source decay kinetics, dead time for event detection, electronic acquisition and time window for coincidence acquisitions including the measurement of delay coincidences (Jan, S. *et al.* 2004), (Cavata-Kerhoas, S. & Guez, D. 2006).

Analytical phantoms can be defined and used with GATE and voxelized sources can be equally employed in order to simulate imaging in realistic conditions (Jan, S. *et al.* 2004).

Time-dependence may be taken into account during all steps of the use of GATE, allowing realistic simulations of the acquisitions counting rates and source decay, and can both be used when defining dynamic configurations (*e.g.* detector movement) (Santin, G. *et al.* 2003).

The geometry description of the microPET<sup>®</sup> scanner is illustrated in Figure 1.

### 2.3 Mouse Phantoms

#### 2.3.1 The MOBY Phantom

In order to simulate data in a realistic way we used a real mouse computer phantom description called MOBY (Segars,

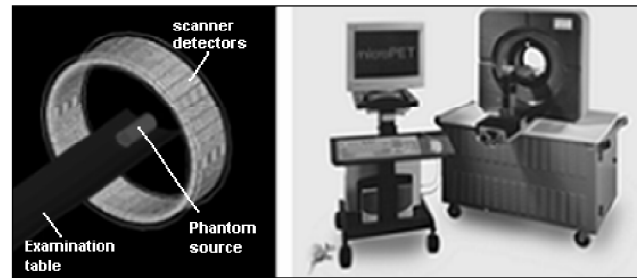


**Figure 1: MicroPET<sup>®</sup> FOCUS 220 geometry modeled by GATE (left) and the real system (right)**

W. P. *et al.* 2004). MOBY combines the realism of a voxelized phantom, with the flexibility of a mathematical phantom based on non-uniform rational B-splines (NURBS). The default whole body MOBY phantom consists of a matrix of  $128 \times 128 \times 448$  cubic voxels with 0.25 mm sides, and is illustrated in Figure 2.

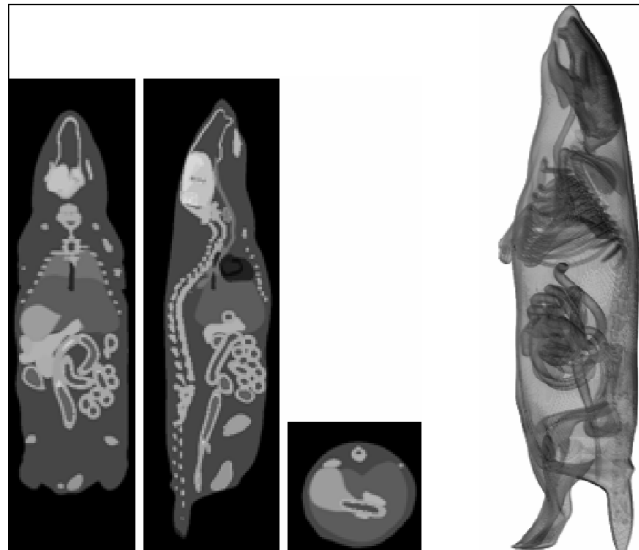


**Figure 2: Coronal, sagittal and transaxial slices corresponding to a PET emission map (left) and illustration of the 511 keV at-tenuation map (right) generated by the MOBY program**

Additionally to a 3D realistic description of the mouse anatomy, the phantom includes 4D models of the mouse's cardiac and respiratory motions. The complete modeling description of organ shapes and cardiac and respiratory motion of MOBY can be found in (Segars, W. P. *et al.* 2004). The respiratory motion in the MOBY phantom is dependent on two time varying parameters: the change in the height of the diaphragm ( $\Delta_{diaphr.}$ ) and the amount of chest expansion ( $\Delta_{Ap}$ ). In the default MOBY configuration, the extent of diaphragmatic motion for normal breathing is set to be 1.0 mm while the chest expansion is 0.7 mm. These values correspond to a respiratory cycle with a period of 0.37 s (Figure 3). These values can be changed to produce different breathing patterns. We have changed the MOBY phantom to reproduce a "stress breathing" condition, in order to mimic

the respiratory mouse motion during a typical PET examination (Figures 3 and 4).

In order to prepare the input data for the simulation, a set of 10 temporal frames of 0.037 s was generated over a complete respiratory cycle. On this configuration the maximum  $\Delta_{diaphr.}(t)$  was set to be 4.2 mm and the maximum  $\Delta_{Ap}(t)$  was defined to be 6.0 mm.

Once these changes were implemented, we applied a resampling procedure on the MOBY matrix and reduced the total number of voxels to  $40 \times 40 \times 124$  voxels which resulted in a voxel unit size of  $0.5 \text{ mm} \times 0.5 \text{ mm} \times 0.5 \text{ mm}$ . This allowed to significantly reduce the computational time needed for simulations and took into account the spatial resolution of the scanner.

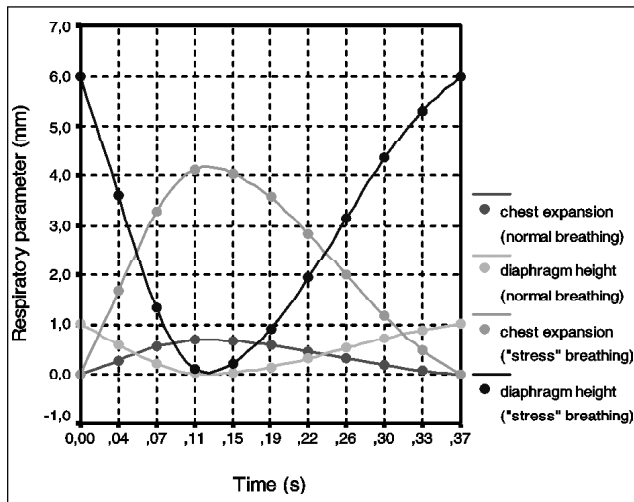


Figure 3: Parameter curves for “normal” and “stress” breathing within MOBY. We used the latest to model respiratory motion in our simulations

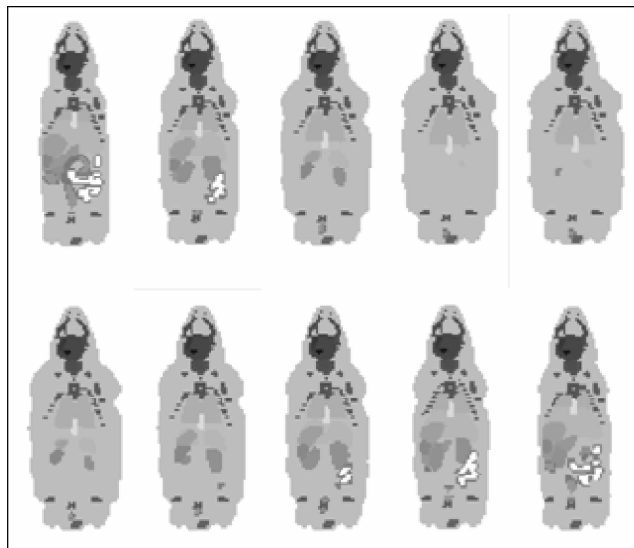


Figure 4: Coronal slices corresponding to the “stress” breathing motion, over one respiratory cycle

### 2.3.2 Phantoms Built from Real Data

The generation of realistic mouse phantoms using real data allowed us to obtain 4D maps of the source distributions,

for the case of the two different radiopharmaceuticals used:  $[^{18}\text{F}]$ fluoride and FDG. Data acquisition were done at CEA/SHFJ (Orsay, France) using a microPET® FOCUS 220 system. Data acquisition protocols were as follows:

2.3.2.1  $[^{18}\text{F}]$ fluoride mouse phantom: Injected activity: 400  $\mu\text{Ci}$ . Acquisition started 20 minutes post injection and lasted 60 minutes. Data was binning as 4 frames of 900 s each. The resulting phantom is illustrated in Figure 5. It consisted of an emission map composed of  $101 \times 55 \times 95$  voxels ( $0.47 \text{ mm} \times 0.47 \text{ mm} \times 0.80 \text{ mm}$ ).

2.3.2.2 FDG mouse phantom: Injected activity: 220  $\mu\text{Ci}$ . Dynamic acquisition lasted 90 minutes. Data was binning as 18 frames ( $5 \times 60\text{s}$ ;  $5 \times 120\text{s}$ ;  $3 \times 300\text{s}$ ;  $3 \times 600\text{s}$ ;  $2 \times 900\text{s}$ ). The resulting phantom is illustrated in Figure 6 and consists of an emission map containing  $104 \times 61 \times 95$  voxels ( $0.46 \text{ mm} \times 0.46 \text{ mm} \times 0.80 \text{ mm}$ ).

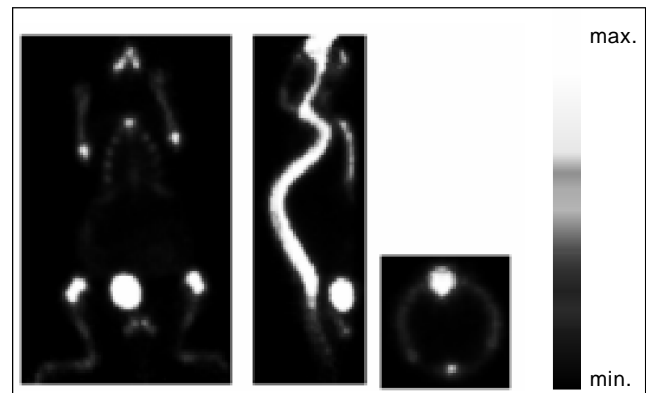


Figure 5: Coronal, sagittal and transaxial slices for the activity distribution of the  $[^{18}\text{F}]$ fluoride mouse phantom

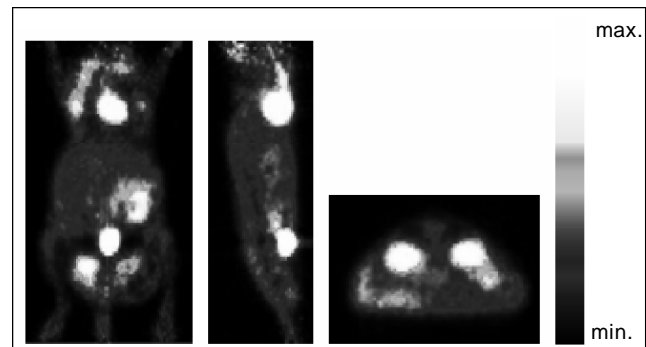


Figure 6: Coronal, sagittal and transaxial slices for the activity distribution of the FDG mouse phantom

Data were reconstructed using the FORE+OSEM2D algorithms (16 subsets and 4 iterations), and corrected for normalization, dead time, scatter and attenuation using the commercial protocols available on the scanner.

## 2.4 Monte Carlo Simulations using GATE

The complete simulation computer platform was installed on a cluster of 512 CPUs with 64 bits architecture operating under a Linux operative system.

The emission map phantoms obtained were used to assign the activity to different anatomical structures. The

simulation parameters were as follows: the energy window was set to 350 keV–750 keV, (representing an energy resolution of 26 % at 511 keV); a coincidence time window of 6 ns including delayed coincidences sorter capability was set; non paralyzable dead time model (both for singles and coincidences) was applied; background noise due to the LSO decay was also included. Positron range, attenuation, scattering and photon acollinearity were not simulated (we used a gamma/gamma emission source). This choice of parameters allowed us to produce simulated data representing an “acquisition best case scenario”. This data can therefore be taken as a gold standard when optimizing image reconstruction and image correction protocols. Simulated data were corrected for detector normalization, rebinned with the Fourier Rebinning algorithm (FORE) and reconstructed using the OSEM2D method (16 subsets and 4 iterations).

As stated above, simulations included two different metabolic models: the  $[^{18}\text{F}]\text{fluoride}$  and the FDG radiotracers. Time dependence was taken into account in all steps of the simulations.

## 2.5 Bone Imaging using $[^{18}\text{F}]\text{fluoride}$

We used the  $[^{18}\text{F}]\text{fluoride}$  mouse exam, described in 2.3.2.1, to set the activity distribution in our simulation studies. This activity was defined using the real whole body mouse exam as reference.

In the case of the  $[^{18}\text{F}]\text{fluoride}$  distribution, only the last acquisition time frame was simulated. This simulation corresponded to a real exam where 284  $\mu\text{Ci}$  are imaged by the microPET<sup>®</sup> FOCUS 220 model during 15 minutes.

Similar simulation conditions were used with the MOBY phantom. In this case, the activity distribution of  $[^{18}\text{F}]\text{fluoride}$  was done according to Table 1. The simulation generated  $4.0 \times 10^{10}$  particles, equivalent to an injected dose of 2.21 mCi imaged during 500 s. This simulation corresponds to an exam where 0.5 mCi are imaged by the microPET<sup>®</sup> FOCUS 220 during 30 minutes.

**Table 1**  
Activity Distribution in the MOBY Phantom at the Last Frame, in the Case of the  $[^{18}\text{F}]\text{fluoride}$

	Activity (Bq/cc)
Body	100.0
Bladder	4000.0
Rib bone	1500.0
Spine bone	1500.0

## 2.6 Metabolic Imaging using FDG

The FDG biodistribution is defined by the TACs which are assigned to different body structures. Figure 7 shows the TACs for each organ obtained for the FDG mouse exam described in the section 2.3.2.2. We have sampled these TACs to set the activity distribution in each organ at each

point in time of our simulations. In order to do this, Regions of Interest (ROIs) were drawn around the bladder, heart, liver, kidneys and whole body. The activity in each ROI was normalized to the total body activity in order to obtain a relative concentration in each organ at each time point.

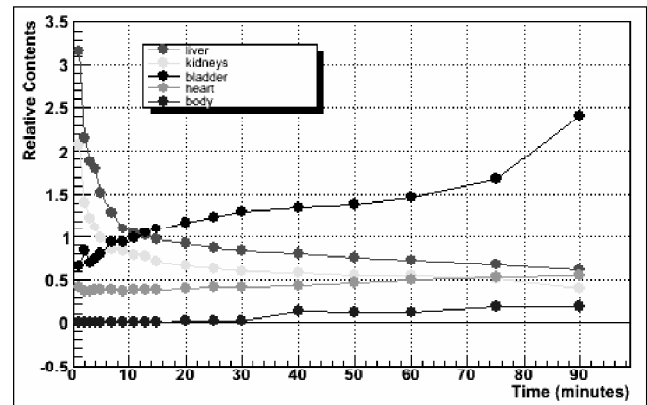


**Figure 7: Measured TACs used as Input in FDG Uptake Simulation**

The defined activity map distribution was set to be representative of real data by assigning minimum and maximum values of measured within a specific body region to intervals of voxel values in the phantom obtained from real data. We simulated an acquisition time of 15 minutes, for an activity of 112  $\mu\text{Ci}$  at the last time frame. This resulted in tracking  $3.5 \times 10^9$  particles within GATE.

A realistic FDG exam simulation was also done using the MOBY phantom. In this case, the emission map used was based on the FDG distribution, as previous stated, at the first and the last time frames of a real exam. For the first frame we simulated 219  $\mu\text{Ci}$  for an acquisition time of 60 s which produced  $4.9 \times 10^8$  particles. We simulated 131  $\mu\text{Ci}$  for  $4.2 \times 10^9$  particles with an acquisition time of 15 minutes, corresponding to the last time frame of the real exam. The activity distribution (input function) for each organ, in each time frame, is shown on Table 2.

**Table 2**  
Input Activity Distribution for the First and the Last Frame in the MOBY Structure for the FDG

	Activity (Bq/cc)	
	First frame	Last frame
Heart	254.7	242.3
Body	0.6	76.3
Liver	1963.3	273.7
Kidneys	1286.1	179.5
Bladder	410.1	1081.4

## 2.7 Including Breathing Mouse on FDG Simulations

We have generated an emission dataset using typical values of FDG uptake for each organ at the last acquisition time frame, for the non normal tidal breathing of the MOBY

phantom described in 2.3.1. No physical effects were taken into account and a back-to-back emission source simulation was performed.

These simulations were computed on a cluster of 10 CPUs during 24 hours, corresponding to an acquisition time of 568.5 s. During this simulation  $3.5 \times 10^8$  particles were generated per each phantom frame (time point in the breathing cycle), corresponding to a total of approximately  $3.5 \times 10^9$  particles.

### 3. RESULTS

#### 3.1 Simulation of [ $^{18}\text{F}$ ] Fluoride Uptake

The simulation of [ $^{18}\text{F}$ ]fluoride uptake using the mouse phantom, built from real data, ran on a computer cluster with 50 CPUs. The computing time was approximately 10 hours. Figure 8 shows representative slices of real and simulated data.

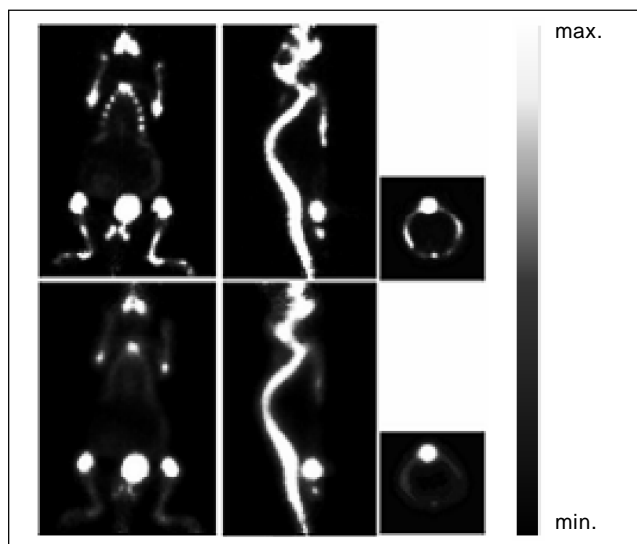


Figure 8: Coronal, sagittal and transaxial slices representing [ $^{18}\text{F}$ ]fluoride uptake: acquired data (top); GATE simulation using the real data phantom as input (bottom)

To validate the accuracy of the simulations quantitative output we compared the real data against the simulated data. We defined ROIs on the bladder, spine bone and rib bone and we normalized the activity concentration in each organ by the total activity uptake, both for real and simulated data. The results obtained after comparing simulated to real data are shown in Figure 9, where the normalized uptake ratios and the standard deviation values measured for each organ (shown as error bars) are represented. The analysis of the relative differences between quantification values obtained for the real and the simulated data show differences of 22.7 % for the bladder; 10.3 % for the spine bone and 13.7 % for the rib bone.

Figure 10 illustrates the cumulated activity obtained by simulation of the [ $^{18}\text{F}$ ]fluoride uptake using the MOBY phantom. The simulation ran on a computed cluster with 50 CPUs and lasted for approximately 21 hours.

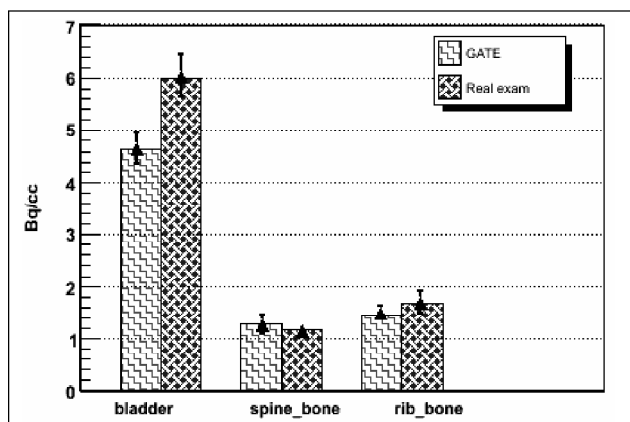


Figure 9: Comparison between PET image quantification and the GATE measurements. Black bars represent the ROI statistical error measured as the ratio standard deviation over mean for all pixels considered



Figure 10: Maximum Intensity Projection (MIP) of the MOBY phantom after a full simulation with an activity distribution representative of the real [ $^{18}\text{F}$ ]fluoride distribution

#### 3.2 Simulation of FDG Uptake

Figure 11 compares two representative images of the mouse FDG distribution obtained from a real examination and from simulation. The simulation ran on a cluster of 10 CPUs with a global computing time of approximately 12 hours.

The accuracy of the quantitative results obtained by simulation was evaluated by comparing simulated data against real data. In order to do this, we defined ROIs on the liver, bladder, heart and kidneys. The values obtained by the use of these ROIs were normalized the activity concentration in each organ by the total activity inside the whole body.

Figure 12 shows the results of this comparison. In this figure, the normalized uptake ratio and the standard deviation measured for each organ (shown as errors bars) are represented. The relative activity concentration obtained for the simulation data are in good agreement with the values obtained for real data.

We have also calculated the relative differences between the quantification values obtained by simulation and with

the real exam. This comparison showed differences of 1.8 % for the liver and the heart; 3.7 % for the bladder and 7.5 % for the kidneys. These differences may partly result from small differences on the ROIs definitions in the real exam and the simulation.

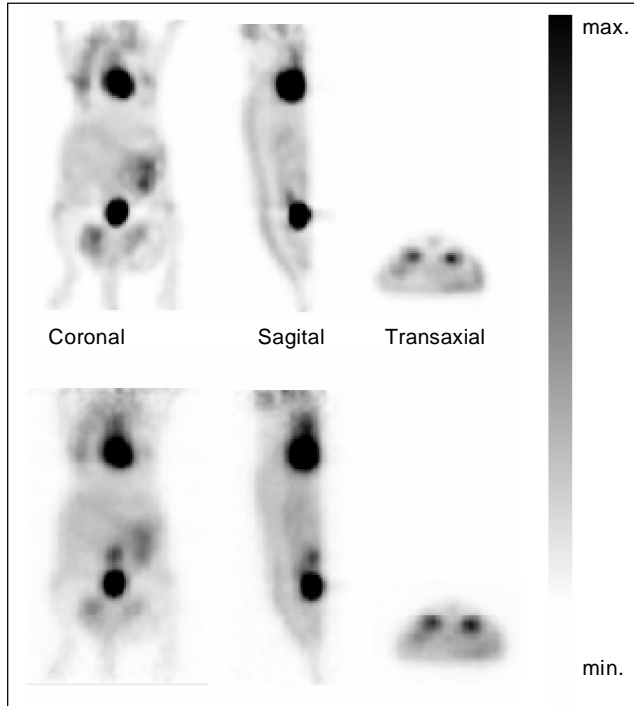


Figure 11: Slices from the real FDG exam (top) and the simulated exam (bottom) for the FDG mouse phantom, with an activity map distribution close to the last activity frame

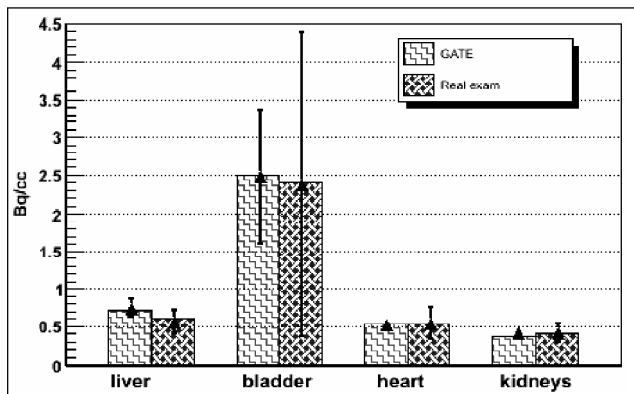


Figure 12: Comparison between PET image quantification and the GATE measurements. Black bars represent the ROI statistical error measured as the ratio standard deviation over mean for all pixels considered

Figure 13 shows the results obtained for the first and the last frames for the FDG simulation using MOBY. These simulations lasted for approximately for 6 hours in the case of the first simulated time frame (using 6 CPUs) and approximately 14 hours for the last time frame (using 10 CPUs).

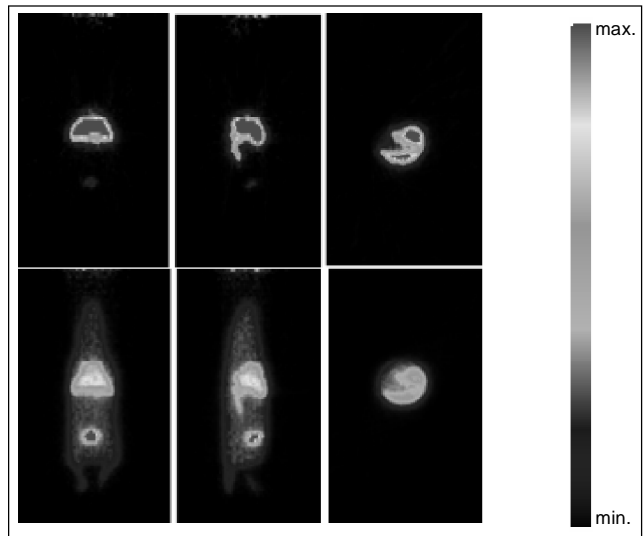


Figure 13: Coronal, sagittal and transaxial slices for FDG simulation using MOBY: top–first activity frame; bottom–last activity frame

### 3.3 Simulation Studies for the FDG Radiotracer Including the Respiratory Motion

The first set of results obtained for the simulation of breathing motion using GATE is shown in Figure 14.

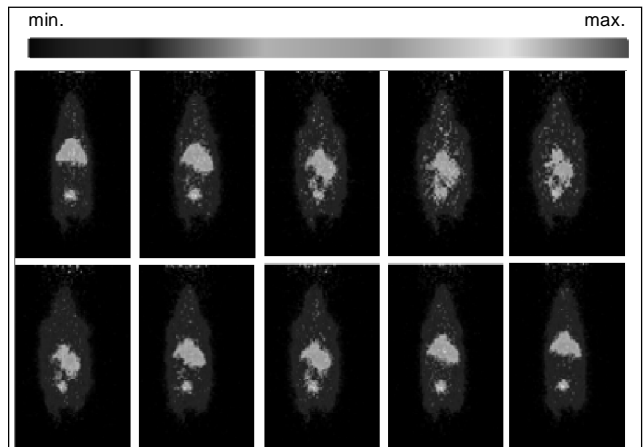


Figure 14: Coronal slices corresponding to the simulation of the breathing motion, over one respiratory cycle for a FDG exam at the last time frame

## 4. DISCUSSION AND CONCLUSIONS

The use of Monte Carlo to simulate new molecular imaging platforms has gathered great interest in the last years. In fact, several groups have presented work on this subject, and particularly on the optimization of imaging instrumentation both in small animal PET and SPECT: (Merheb, C. *et al.* 2007), (Jan, S. *et al.* 2006), (Sakellios, N. *et al.* 2006), (Karakatsanis, N. *et al.* 2006), (Schmidlein, C. R. *et al.* 2006), (Lamare, F. *et al.* 2006), (Rannou, F. R. *et al.* 2004), (Vandervoort, E. *et al.* 2005), (Bataille, F. *et al.* 2004), (Simon, L. *et al.* 2004), (Lazaro, D. *et al.* 2004) among other publications and some in dosimetry applications: (Visvikis,

D. *et al.* 2006a), (Taschereau, R. *et al.* 2006), (Taschereau, R. & Chatziioannou, A. F. 2005). Some other groups have also presented preliminary work on the use of the Monte Carlo method to simulate breathing motion on human models: (He, J. *et al.* 2006), (Zhu, Z. Z. *et al.* 2003). Nevertheless, these groups did not study in detail the problem of simulating realistic metabolic small animal exams using GATE.

In this paper, we presented the first results on the realistic simulation of small animal metabolic studies using the microPET® FOCUS 220 system and a first preliminary approach of Monte Carlo simulation studies for the FDG radiotracer using the MOBY phantom including respiratory motion. The work presented reflects the potential of using GATE to simulate small animal exams and exempts the obtained results from effects related to the image reconstruction algorithms used (they were the same for real and simulated data) and physical effects (they were corrected on real images and they were not simulated on GATE).

We chose to use a two-fold approach on our simulations. On one hand, we have built realistic phantoms from real data and on the other we have used a voxelized realistic mouse phantom, MOBY. Comparing the output of the simulations with real data allowed us to evaluate the limitations of using GATE with both strategies. An important aspect of simulation is to have a realistic model (phantom) of the subject's anatomy and physiological functions from which imaging data can be generated using accurate models of the imaging process. The advantage in using such phantoms in simulation studies is that the exact anatomy and physiological functions are known. Moreover, computer phantoms can be altered in order to model different anatomies and pathological situations.

In the first part of this paper we produced Monte Carlo simulations for the [ $^{18}\text{F}$ ]fluoride radiotracer for both the generated mouse phantom from acquired data and the MOBY phantom. The [ $^{18}\text{F}$ ]fluoride tracer normally accumulates at the bones and highlights the skeletal system of the animal. Simulations performed reproduce the same pattern. Furthermore, the relative activity concentrations for the simulation data are in good agreement with the same measurements for the real values. The analysis of the relative differences between quantification values obtained for the real and the simulated data that may in part result from small differences on the definition of ROIs between real and simulated data. Even so, the maximum difference obtained is 22.7% in the case of the bladder. Additionally, the calculated standard deviation, related to the quantification analysis, show that the variability from simulated results is lower than the measurements obtained from the real exams. This difference most probably results from a sub-optimal correction of these effects on real data.

At the second part of this paper we have simulated small animal metabolic imaging using FDG. FDG is taken up by cells to the same extent as glucose but is not metabolized.

Evident accumulation of FDG in the mouse body can be seen *in vivo* especially in the brain, heart, kidneys and bladder 60 minutes after injection. Unlike glucose, FDG is excreted by the kidneys into the bladder.

We have simulated the first and the last time frames of an FDG dynamic exam, using the MOBY phantom, in order to evaluate the uptake variability of the tracer during the exam. As we saw, the differences between the activity distribution for the liver and the heart are very small, disabling a clear separation between the two organs. This fact results from the specific description of the organs inside the MOBY phantom, since in MOBY the liver lies slightly in front of the hearth. Although, the activity simulated distribution are in good agreement with the FDG biodistribution. In the last frame it is possible to see higher accumulated activity inside the bladder, compared with the first frame, something which is expected in a usual dynamic FDG exam.

The accuracy of the quantitative results obtained by simulations was evaluated by comparing simulated data against real data, for the simulation with the acquired mouse phantom. The relative activity concentration obtained for the simulation data are in good agreement with the values obtained for real data. As for the case of [ $^{18}\text{F}$ ]fluoride, the calculated standard deviation, related to the quantification analysis, show that the variability from simulated results is lower than the measurements obtained from the real exams. This difference most probably results from a sub-optimal correction of these effects on real data.

Overall, the good agreement between simulation and the real acquisitions leads us to conclude that GATE platform is an important tool to perform mouse PET imaging simulation when assessing [ $^{18}\text{F}$ ]fluoride and FDG distributions. Moreover, we showed a first preliminary approach of Monte Carlo simulation studies for the FDG radiotracer using the MOBY phantom which include respiratory motion.

In spite the encouraging results obtained, this study has several limitations. The simulations are generally long and difficult to perform without a very well equipped computer structure. The production of the realistic images, including attenuation information (using the phantoms attenuation maps to set the different body structures and the correspondent attenuation information) and physical effects (using the isotope decay instead a gamma/gamma emission source), was not done. Although this was not among the main goals of this work, its inclusion will allow evaluating the consequence of these physical effects on image sensitivity and quantification. Additionally, the use of realistic phantoms generated from acquired data results on visual differences between the image resolution of real data and simulated data. These differences are due to the presence of an additional image blurring on simulated data, resulting from the fact that its input already reflects all the image acquisition and processing chain characteristic of the scanner used.

This work is being complemented by accessing the impact of such motion in the detection of lung lesions (including lesion movement as a function of respiratory motion). In fact, recent studies have shown that respiratory gating can provide more accurate definition on the lesion volume and improves the image quantification (Sadek, A. *et al.* 2002), (Visvikis, D. *et al.* 2006b). To reduce the blurring, due to the respiratory motion, it is possible to use the respiratory gating method. In order to contribute to the full understanding of this problem, this work is being complemented by accessing the impact of such motion in the detection of lung lesions (including lesion movement as a function of respiratory motion). This includes developing dynamic simulations using the MOBY phantom, which take into account the mouse breathing motion and the simulation of the FDG uptake in a lung tumor model. It is known that the localization and detection of lesions in thoracic and abdominal imaging is often affected by the respiratory motion due the displacement of the organs during normal breathing. Since there are many variables involved on the used of this method, which affect the performance of the gating studies, are needed to provide an approach for optimal gating scheme in FDG lung PET imaging. The use of the dynamic respiratory feature available in the MOBY model will allow an initial investigation on the impact of respiratory motion on lesion detection for FDG PET exams. Studies of the effects of the respiratory motion under several gating schemes will be performing.

In the near future, realistic dynamic simulations with different radiotracers, such as the *3-Deoxy-<sup>18</sup>F*fluorothymidine (FLT) or *[<sup>11</sup>C]raclopride*, will be done. Biological kinetics using compartmental modeling will also be implemented within the GATE platform.

As a final conclusion, we may state that the results presented in this paper show that GATE is well suited to model the microPET<sup>®</sup> FOCUS 220 system for quantitative analysis and to implement realistic voxelized whole body mouse phantoms. We have shown that the GATE platform can simulate small animal PET acquisitions under realistic conditions. These simulations may be useful to improve the quantitative analysis of whole body mouse studies. In the medium term they are expected to play a significant role in designing and optimization of clinical protocols in Positron Emission Tomography.

#### REFERENCES

- [1] Agostinelli, S. *et al.* Geant4 – a simulation toolkit. *Nuclear Instruments and Methods in Physics Research A* 506: 250-303, (2003).
- [2] Andreo, P., Monte Carlo techniques in medical radiation physics. *Physics in Medicine and Biology* 36(7): 861-920, (1991).
- [3] Bataille F. *et al.*, Monte Carlo Simulation for the ECAT HRRT using GATE. *2004 IEEE Nuclear Science Symposium Conference Record, Rome, 16-22 October, 2004*: 2570-2574, (2004).
- [4] Berger, F. *et al.*, Whole-body skeletal imaging in mice utilizing microPET: optimization of reproducibility and applications in animal models of bone disease. *European Journal of Nuclear Medicine* 29(9): 1225-1236, (2002).
- [5] Branco, S., Jan, S. and Almeida, P. 2007a. Monte Carlo Simulations in Small Animal PET Imaging [Imaging 2006 conference Proceeding]. *Nuclear Instruments and Methods in Physics Research A, Stockholm, 27-30 June, 2006* (in press).
- [6] Branco, S., Jan, S. and Almeida, P. 2007b. Molecular Imaging of Small Animals PET using Monte Carlo Simulations. *Revista do Departamento de Electrónica, Telecomunicações e Informática da Universidade de Aveiro* 4(7): 845-848.
- [7] Branco, S., Jan, S. and Almeida, P. 2007c. Monte Carlo Simulations Studies in Small Animal PET. *Proceedings of the International Symposium CompIMAGE 2006, Coimbra, 20-21 October, 2006*: 111-115.
- [8] Cavata-Kerhoas, S. & Guez, D., Modeling electronic processing in GATE. *Nuclear Instruments and Methods in Physics Research A* 569: 330-334, (2006).
- [9] Chatziioannou, A. F., PET Scanners Dedicated to Molecular Imaging of Small Animal Models. *Molecular Imaging and Biology* 4(1): 47-63, (2002).
- [10] Cherry, S., *In vivo* molecular and genomic imaging: new challenges for imaging physics. *Physics in Medicine and Biology* 49: R13-R48, (2004).
- [11] Cherry, S. R. & Gambhir S. S., Use of Positron Emission Tomography in Animal Research. *Institute for Laboratory Animal Research Journal* 42(3): 219-232, (2001).
- [12] Couturier, O., Fluorinated tracers for imaging cancer with positron emission tomography. *European Journal of Nuclear Medicine and Molecular Imaging* 31(8): 1182-1206, (2004).
- [13] Gambhir, S. S., Molecular Imaging of Cancer with Positron Emission Tomography. *Nature Reviews* 2: 683-693, (2002).
- [14] He, J. *et al.*, The Application of GATE and NCAT to Respiratory Motion Simulation in Allegro PE. *2006 IEEE Nuclear Science Symposium Conference Record, San Diego, 29 October-4 November, 2006*: 2589-2593, (2006).
- [15] Jan, S. *et al.*, GATE: a simulation toolkit for PET and SPECT. *Physics in Medicine and Biology* 49(19): 4543-4561, (2004).
- [16] Jan, S. *et al.*, Monte Carlo Simulations of the microPET FOCUS system for small rodents imaging applications. *2005 IEEE Nuclear Science Symposium Conference Record, Puerto Rico, 23-29 October, 2005*: 1653-1657, (2005).
- [17] Jan, S. *et al.* 2006. Monte Carlo database production for human brain PET imaging using GATE. *2006 IEEE Nuclear Science Symposium Conference Record, San Diego, 29 October-4 November, 2006*: 3159-3162.
- [18] Karakatsanis, N. *et al.*, Comparative evaluation of two commercial PET scanners, ECAT EXACT HR+ and Biograph 2, using GATE. *Nuclear Instruments and Methods in Physics Research A* 569: 368-372, (2006).
- [19] Lamare, F. *et al.*, Validation of a Monte Carlo simulation of the Philips Allegro/GEMINI PET systems using GATE. *Physics in Medicine and Biology* 51: 943-962, (2006).
- [20] Larson, S. M. & Schwartz, L. H., <sup>18</sup>F-FDG PET as a candidate for “Qualified Biomarker”: Functional Assessment of Treatment Response in Oncology. *The Journal of Nuclear Medicine* 47(6): 901-903, (2006).
- [21] Lazaro, D. *et al.*, Validation of the GATE Monte Carlo simulation platform for modeling a CsI(Tl) scintillation camera dedicated to small-animal imaging. *Physics in Medicine and Biology* 49: 271-285, (2004).

- [22] Luanne, L. P. *et al.*, The mouse as a model for human biology: a resource guide for complex trait analysis. *Nature Reviews* 8: 58-69, (2007).
- [23] Merheb, C. *et al.*, Full modelling of the MOSAIC animal PET system based on the GATE Monte Carlo simulation code. *Physics in Medicine and Biology* 52: 563-576, (2007).
- [24] Phelps, M. E., Positron emission tomography provides molecular imaging of biological processes. *Proceedings of the National Academy of Sciences of the United States of America* 97(16): 9226-9233, (2000).
- [25] Rannou, F. R. *et al.*, Investigation of OPET Performance Using GATE, a Geant4-Based Simulation Software. *IEEE Transactions on Nuclear Science* 51(5): 2713-2717, (2004).
- [26] Sadek, A. *et al.*, Effect of Respiratory Gating on Quantifying PET Images of Lung Cancer. *The Journal of Nuclear Medicine* 43(7): 876-881, (2002).
- [27] Santin, G. *et al.*, GATE: A Geant4-based simulation platform for PET, SPECT integrating movement and time management. *IEEE Transactions on Nuclear Science* 50: 1516-1521, (2003).
- [28] Schmidlein, C. R. *et al.*, Validation of GATE Monte Carlo simulations of the GE Advance/Discovery LS PET scanners. *Medical Physics* 33(1): 198-208, (2006).
- [29] Segars, W. P. *et al.*, Development of a 4-D Digital Mouse Phantom for Molecular Imaging Research. *Molecular Imaging and Biology* 6(3): 149-159, (2004).
- [30] Simon, L. *et al.*, Simulation of time curves in small animal PET using GATE. *Nuclear Instruments and Methods in Physics Research A* 527: 190-194, (2004).
- [31] Taschereau, R. & Chatziioannou, A. F. 2005. FDG-PET Image-based Dose Distribution in a Realistic Mouse Phantom from Monte Carlo Simulations. *2005 IEEE Nuclear Science Symposium Conference Record, Puerto Rico, 23-29 October, 2005: 1633-1636.*
- [32] Taschereau, R. *et al.*, Monte Carlo simulations of dose from microCT imaging procedures in a realistic mouse phantom. *Medical Physics* 33(1): 216-224, (2006).
- [33] Tai, Y. C. & Laforest, R., Instrumentation Aspects of Animal PET. *Annual Review of Biomedical Engineering* 7: 255-285, (2005).
- [34] Tai, Y. *et al.*, Performance Evaluation of the microPET FOCUS: A Third-Generation microPET Scanner Dedicated to Animal Imaging. *Journal of Nuclear Medicine* 46: 455-463, (2005).
- [35] Vandervoort, E. *et al.*, Monte-Carlo modeling of the microPET R4 small animal PET scanner for coincidence-mode emission and singles-mode transmission data acquisition. *2005 IEEE Nuclear Science Symposium Conference Record, Puerto Rico, 23-29 October, 2005: 2449-2453, (2005).*
- [36] Visvikis, D. *et al.*, Use of GATE Monte Carlo package for dosimetry applications. *Nuclear Instruments and Methods in Physics Research A* 569: 335-340, (2006a).
- [37] Visvikis, D. *et al.*, Respiratory motion in positron emission tomography for oncology applications: Problems and Solutions. *Nuclear Instruments and Methods in Physics Research A* 569: 453-457, (2006b).
- [38] Wernick, M. N. & Aarsvold, J. N., *Emission Tomography: The Fundamentals of PET and SPECT*. California: Elsevier Academic Press, (2004).
- [39] Zaidi, H., Relevance of accurate Monte Carlo modeling in nuclear medical imaging. *Medical Physics* 26(4): 574-608, (1999).
- [40] Zhu, Z. Z. *et al.*, A Simulation Study of the Effect of Gating Scheme on Respiratory Motion Blurring in FDG Lung PET. *2002 IEEE Nuclear Science Symposium Conference Record, Norfolk, 10-16 November, 2002: 1554-1558, (2003).*